Low-temperature domain-wall freezing and nonequilibrium dynamics in the transverse-field Ising model material $CoNb_2O_6$

C. L. Sarkis [1], S. Säubert [1], V. Williams,[1] E. S. Choi,[2] T. R. Reeder,[3] H. S. Nair [4], and K. A. Ross[1,5,*]

[1]*Department of Physics, Colorado State University, 200 West Lake Street, Fort Collins, Colorado 80523-1875, USA*

[2]*National High Magnetic Field Laboratory, Florida State University, Tallahassee, Florida 32310-3706, USA*

[3]*Department of Physics and Astronomy and Institute for Quantum Matter, Johns Hopkins University, Baltimore, Maryland 21218, USA*

[4]*Department of Physics, University of Texas El Paso, 500 West University Avenue, El Paso, Texas 79902, USA*

[5]*Quantum Materials Program, CIFAR, MaRS Centre, West Tower 661 University Avenue, Suite 505, Toronto, Ontario, M5G 1M1 Canada*

$CoNb_2O_6$ is a rare realization of the transverse-field Ising model, making it a useful tool for studying both equilibrium and nonequilibrium many-body quantum physics. Despite a large body of work dedicated to characterizing this material, details of the ordered states in the presence of relatively weak transverse fields have not been discussed in detail. Here, we present a detailed study of $CoNb_2O_6$ via ac susceptibility measurements in order to further characterize its low-temperature behavior in the presence of a transverse field. Specifically, we call attention to an unconventional freezing transition in zero field below $T_F = 1.2$ K, occurring *within* the well-known commensurate antiferromagnetic (CAFM) state that onsets at $T_{N2} = 1.9$ K. We performed a series of transverse-field quenches into this frozen state, which resulted in a slowly relaxing susceptibility, $\chi'(t)$, that followed a logarithmic decay within the time range measured. We discuss the frozen state in the context of the freezing of previously discussed "free" chains arising from domain walls between the four degenerate sublattices of the CAFM state. We also attempted to observe Kibble-Zurek scaling by quenching the transverse field into the frozen state at different rates. This produced a null result; the behavior can be fully explained by coarsening of domains over the time scale of the quenches. The absence of a clear Kibble-Zurek scaling is itself surprising, given the proposed ubiquity of the phenomenon for general second-order phase transitions.

I. INTRODUCTION

Recently nonequilibrium condensed matter has become a prominent field of study as a generator of exotic phenomena, such as many-body localization [1–3] and Kibble-Zurek scaling [4–6]. While theory has been propitious in some areas, much progress in nonequilibrium relies heavily on the guidance of experiment. Thus, experimental studies which are centered on tractable models are crucial for the field of nonequilibrium physics.

One of the archetypal models of condensed matter is the transverse-field Ising model (TFIM) [7–9],

$$H = J \sum_{\langle i,j \rangle} \sigma_i^z \sigma_j^z - h_x \sum_i \sigma_i^x, \quad (1)$$

where σ_i^α ($\alpha = x, y, z$) are Pauli spin matrices, J is the exchange interaction strength, and h_x represents an external magnetic field transverse to the Ising (z) axis. This model can be exactly solved in one dimension and features a quantum critical point at $J = 2h_x$ [7,9]. The TFIM provides a robust theoretical framework to study quantum criticality and nonequilibrium many-body physics.

While real material analogs of the TFIM with critical fields accessible in current laboratory settings are rare, one

key example is the quasi-one-dimensional (1D) Ising material $CoNb_2O_6$. This material was extensively studied from the 1970s to the 2000s, with the goal of characterizing its complex magnetic phase diagram in the presence of a magnetic field [10–16], though the *transverse-field* behavior was not investigated until later [17]. The electronically insulating $CoNb_2O_6$ crystallizes into the orthorhombic columbite space group *Pbcn*, with room-temperature lattice parameters of $a = 14.1475$ Å, $b = 5.712$ Å, and $c = 5.045$ Å [18]. The Co^{2+} sublattice is shown in Fig. 1(a). Co^{2+} ions are linked by oxygen octahedra forming zigzag chains along the c axis, with ~90° superexchange giving rise to ferromagnetic nearest-neighbor interactions J_0 and a pronounced 1D behavior [19]. Staggered planes of isosceles triangles form in the ab plane, with antiferromagnetic (AFM) interactions $|J_1| > |J_2|$ between chains estimated to be an order of magnitude smaller than J_0 [20]. The isosceles triangular arrangement combined with AFM Ising interactions results in geometric frustration, which, when combined with the 1D magnetism of the chains and strongly Ising-like interactions, leads to a complex magnetic phase diagram that strongly depends on the field direction [13,21,22]. In zero field, the system undergoes a phase transition at $T_{N1} = 2.9$ K into an incommensurate AFM (ICAFM) phase with temperature-dependent wave vector $q = (0\,q_y\,0)$. Below $T_{N2} = 1.9$ K, the system locks into a commensurate AFM (CAFM) phase with $q = (0\,0.5\,0)$ via a first-order phase transition. Within the CAFM phase, neutron
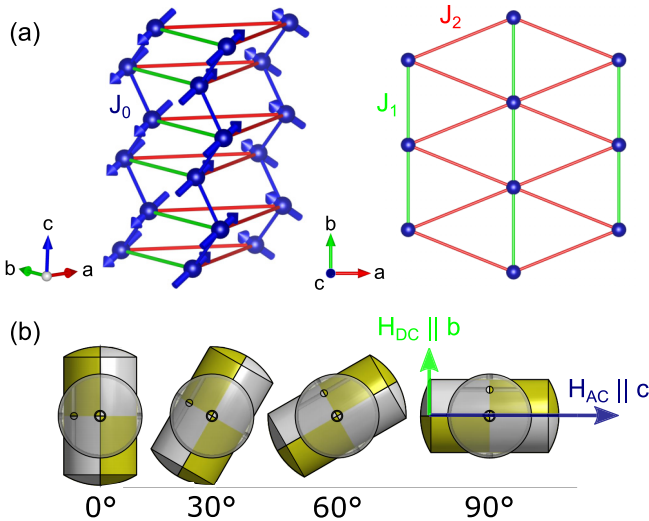
*kate.ross@colostate.edu

FIG. 1. (a) Magnetic structure of $CoNb_2O_6$ in the CAFM state. Nearest neighbors form zigzag chains along c with ferromagnetic interactions (J_0). Second (J_1) and third (J_2) neighbors (both AFM) connect isosceles triangles in the ab plane which stabilize 3D order at low temperatures. J_0 is roughly an order of magnitude larger than the other exchange interactions, making $CoNb_2O_6$ quasi-1D. (b) Diagram of the ac susceptometer at the NHMFL, showing the directions of the ac and dc fields. The ac field can be set at any angle with respect to the dc field, within a single plane of rotation. For our experiments, the ac field was oriented along the c axis (the average Ising direction), and the dc field was usually oriented along the b axis (transverse to the Ising axes).

diffraction showed that $CoNb_2O_6$ has an ordered moment of $\mu \approx 3.2\mu_B$ [14]. Heat capacity measurements showed that magnetic contributions persist up to $T = 25$ K [13] and have an associated entropy of $R\ln 2$, supporting an $S_{eff} = \frac{1}{2}$ picture for the low-temperature angular momentum degrees of freedom [13,23]. In the CAFM state, there are two local moment directions, canted $\pm 31°$ away from the c axis and lying within the ac plane. A series of papers by Kobayashi *et al.* reported anisotropic domain coarsening within the ab plane (the triangular network) at $T = 1.5$ K exhibiting an anomalously small growth exponent of $n = 0.2$ [24,25]. This low growth exponent was attributed to the effects of frustration.

More recently, there has been renewed interest in $CoNb_2O_6$ due to its application in the TFIM [21]. Neutron scattering under a transverse field (i.e., applied along the b axis) revealed an emergent $\mathbb{E}_8$ symmetry [17], which describes the 1D transverse-field Ising chain at the quantum critical point with small but finite longitudinal field [21,26–28]. Transverse-field heat capacity [23] and nuclear magnetic resonance [29] measurements revealed that the quantum phase transition (QPT) for an isolated Ising chain in $CoNb_2O_6$ would be at 5.25 T; however, this is buried within the three-dimensional (3D) ordered phase which exhibits a QPT at 5.45 T [22], due to weak but nonzero interchain couplings. Recently it has been argued that additional off-diagonal exchange interaction terms are important for a quantitative understanding of $CoNb_2O_6$ [30,31], implying that the symmetry is not strictly Ising like. Even so, the field-induced quantum critical point of the proposed models still maps onto the TFIM [30]. Given how well

studied the material now is due to its behavior in a transverse field, there is a surprising lack of detail in the literature about its response to low transverse-field strengths. In order to use $CoNb_2O_6$ to experimentally investigate nonequilibrium properties of the TFIM, it is important to fully characterize its low-temperature and low-transverse-field magnetic properties, particularly since they exhibit slow relaxation in this regime.

Here, we report ac susceptibility measurements on $CoNb_2O_6$ taken down to a temperature of $T = 0.5$ K. We used a transverse dc field geometry [Fig. 1(b)] to measure the ac susceptibility along the c axis in various scenarios: (1) the zero-field ac susceptibility, (2) the ac susceptibility as a function of transverse field, and (3) the relaxation of the ac susceptibility in zero field after ramping the transverse magnetic field to zero at various rates (r_Q), spanning 0.1–10 T/min. For the zero-field data we find good agreement with prior measurements [13], including the presence of a freezing transition which onsets at $T_F \sim 1.2$ K in our sample. This freezing transition, which occurs within the commensurate ordered phase, is not usually discussed in studies of $CoNb_2O_6$, but appears to be present in several samples [12,13,20,23]. The transverse-field dependence of the ac susceptibility at 0.5 K reveals several features which can be identified as transitions between different ordered states, culminating in the 3D quantum critical point (QCP) at 5.45 T. Upon quenching the transverse field into the frozen state, we observe a relaxation in the real $[\chi'(t)]$ and imaginary $[\chi''(t)]$ components of the ac susceptibility, which is best described by a logarithmic decay. This contrasts with the power-law relaxation of ac susceptibility (and neutron Bragg diffraction) that was found by Kobayashi *et al.* at $T = 1.5$ K after longitudinal (c-axis) field quenches [24,25], and points to the role of a disordered potential leading to modified coarsening behavior below T_F. Varying the quench rate (r_Q) of the transverse field, we also find a logarithmic dependence of χ' on r_Q. Though the scaling could also be fit fairly well to a power law, which would suggest a connection to the Kibble-Zurek mechanism (KZM), we find that the dependence can be attributed entirely to a systematic effect resulting from the relaxing population of domain walls over the course of the quench time. This highlights the care necessary in showing KZM behavior for experimental systems in which coarsening occurs on a similar time scale to the quench time [32,33]. It appears that KZM is not evident in our measurements, which in itself is surprising given the ubiquitous nature of the mechanism for second-order transitions [4,6] and glass transitions [34,35].

II. EXPERIMENTAL METHODS

Small single crystals of $CoNb_2O_6$ ($2 \times 1 \times 0.5$ mm) were prepared via flux growth, following Ref. [36], using 1.5 g $CoNb_2O_6$ with 1 g borax ($Na_2B_4O_7$) in a Pt crucible (1250 °C for 15 h then 750 °C for 12 h with temperature ramps of 1.2 K/h). Representative samples were crushed and checked for phase purity with an x-ray powder diffractometer. Alignment and crystallinity were checked with a Laue diffractometer, where the crystal was aligned within $\sim 0.5°$. Two single crystals were used for ac susceptibility with masses of 13.6 and 8.2 mg, both cut into a cuboidal shape.
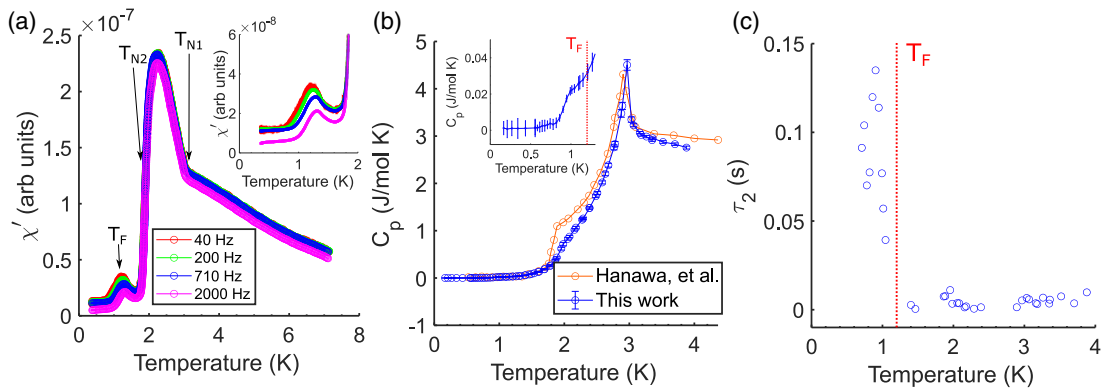
FIG. 2. (a) Zero-field susceptibility of $CoNb_2O_6$ as a function of probe frequency. A frequency-dependent peak is seen centered around $T_F \sim 1.2$ K (shown in inset), consistent with Ref. [13]. (b) Single-crystal heat capacity of $CoNb_2O_6$. A sharp peak at $T_{N1} = 2.9$ K coincides with the ICAFM transition, while a broad shoulder at $T_{N2} = 1.9$ K coincides with the CAFM transition. Heat capacity from Ref. [13] is also shown here in order to highlight the overall agreement between measurements. Inset: A small shoulder is observed in the heat capacity near $T = 1$ K, which could be due to the freezing transition observed in the zero-field susceptibility. (c) Dependence of τ_2 on temperature, which is a measure of the sample-to-stage relaxation processes. τ_2 becomes nonzero near the onset of the frequency-dependent low transition found in zero-field ac susceptibility.

Heat capacity measurements on a small single crystal (1.55 mg) grown from the same batch were performed in zero field from 4 to 0.06 K. The data were taken in a Quantum Design Dynacool Physical Property Measurement System with dilution refrigerator insert using the thermal relaxation method.

Transverse-field ac susceptibility data were taken at the National High Magnetic Field Laboratory (NHMFL) in Tallahassee with a ^{3}He cryostat mounted in a 20-MW 31-T 50-mm bore resistive solenoid dc magnet [37]. The samples were subjected to both an ac and dc field, and were oriented such that the ac field was applied along the average moment direction (c axis), while the dc field could be oriented anywhere within the bc plane, i.e., between the average moment direction and the transverse direction [Fig. 1(b)]. The ability to change the angle *in situ* enabled us to more accurately align the dc field to the b axis within the plane of rotation, by observing the symmetry of the ac signal as a function of rotation angle (Appendix B). The resistive magnet allowed for linear magnetic field ramps of the dc field with rates up to 10 T/min (note that a typical maximum ramp rate for a superconducting magnet is $\leqslant 1$ T/min, which is what motivated us to use a resistive magnet instead). The ac field had amplitude 1.65 Oe and frequencies ranging between $f = 40$ Hz and 10 kHz, with most dc field-dependent measurements taken at 710 Hz. The dc field-dependent data were collected at $T = 0.5$ K with high-temperature background scans taken at $T = 10$ K.

III. RESULTS AND DISCUSSION

A. Temperature dependence of zero-field susceptibility

The zero-field ac susceptibility data are shown in Fig. 2(a). A kink in the susceptibility at $T_{N1} = 2.9$ K coincides with the ICAFM transition. An abrupt decrease in susceptibility is observed at the CAFM transition, $T_{N2} = 1.9$ K. $CoNb_2O_6$ shows a pronounced frequency dependence below $T_F = 1.2$ K accompanying a small peak in the susceptibility. This feature was also observed by Hanawa *et al.* in their ac suscepti-

bility data, who attributed it to a metamagnetic (first-order) transition and noted that it did not appear when measuring along the crystallographic b axis [13]. The CAFM order is known to persist to 0.05 K [22], so this frequency-dependent feature appears to signal a frozen state that coexists with the CAFM state.

The heat capacity of $CoNb_2O_6$ in zero field is shown in Fig. 2(b), which agrees well with the literature [13,23]. A sharp anomaly corresponds to T_{N1}, while a low-temperature shoulder corresponds to T_{N2}. A second smaller shoulder is also observed around 1 K, which may be related to the freezing transition discussed above. Significant magnetic heat capacity remains above the transitions and is known to persist to ~ 25 K [13], well within the paramagnetic state, revealing the presence of short-range spin correlations up to this temperature. The thermal relaxation method allows one to analyze the relaxation curves in terms of a two-time-constant model, where τ_1 is related to the heat capacity of the sample, and τ_2 is related to the heat flowing from within the sample to the sample platform and can be an indicator for slow relaxation within the sample [38,39]. The onset of significant τ_2 at $T \sim 1.2$ K [shown in Fig. 2(c)] is consistent with slow thermal relaxation within the sample, as expected based on the zero-field limit of the freezing transition revealed by ac susceptibility at the same temperature.

Previous studies by Kobayashi *et al.* have also shown slow relaxation in $CoNb_2O_6$ within the CAFM phase, but at temperatures above the freezing transition that we report [24,25]. In those studies, the ferromagnetic (FM) c-axis chains were treated as single superspins (since J_0 is by far the dominant exchange interaction, the spins along each chain were assumed to have the same orientation), and the defects of the ordering of those superspins within the ab plane were investigated. The CAFM state in $CoNb_2O_6$ has a fourfold degeneracy, so domains of this order populate randomly following a quench into the ordered state, with domain walls forming between them. Kobayashi *et al.* deduced the presence of "free" chains at certain types of domain walls, which arise due to the

frustration of the isosceles triangular lattice formed by the chains. A time dependence of both the correlation length and the magnetic susceptibility was also reported in Ref. [25] at $T = 1.5$ K, just above the T_F. In that study, the relaxation behavior was modeled by a power law, consistent with domain-coarsening theory. However, the growth exponent was found to be anomalously low ($n = 0.20 \pm 0.02$), in contrast to standard coarsening models of a fourfold-degenerate Ising system with curvature-driven domain growth, which predict a growth exponent of $n = 0.5$ [40,41], though within the anisotropic nearest-neighbor Ising (ANNNI) model used in Ref. [25] deviations from this exponent have been predicted [42].

One possible explanation for the freezing transition we observed within the CAFM state is the influence of disorder on the domain-wall dynamics discussed above. A natural route to disorder in $CoNb_2O_6$ comes from the CoO-Nb_2O_5 binary phase diagram [43], which shows that $CoNb_2O_6$ is not a "line compound"; i.e., there is a fairly wide range of stoichiometries (within ∼1% of the ideal 1:1 molar ratio) that lead to the same average crystal structure (the columbite structure type). The relatively wide compositional space that stabilizes the columbite structure indicates a low enthalpy for defects relative to the concomitant gain in configurational entropy (e.g., antisite disorder or vacancies). Thus, even for perfect stoichiometry, one could expect a relatively high defect density [44,45]. It is already known that $CoNb_2O_6$ can be extremely sensitive to small amounts of disorder [46,47]; for instance, in $Mg_xCo_{1-x}Nb_2O_6$, less than 1% substitution ($x = 0.008$) is enough to entirely suppress the CAFM state at low temperatures [47]. Given this sensitivity to small amounts of disorder, one may wonder how general or sample dependent the low-temperature phase in $CoNb_2O_6$ is. Along with the observation by Ref. [13], we have observed the feature in multiple crystals grown through two separate techniques: flux growth and optical floating zone. We are thus inclined to believe such a freezing transition is a general feature in $CoNb_2O_6$, although whether it is intrinsic to the low-temperature state of the system itself or simply related to the inclusion of disorder is an open question worthy of future study.

B. Transverse-field dependence of susceptibility

Typical ac susceptibility data taken as a function of field at constant temperature (0.5 K) are shown in Fig. 3. The data were taken after cooling in zero field from 2 to 0.5 K. Features in these data align well with phase transitions identified from neutron-scattering data [22] and are indicated in the figure by arrows. A shoulder near 5.3 T shows the transition between an ordered state and a field-polarized paramagnet, with a small accompanying hysteresis between ramps of increasing and decreasing field. The hysteresis is more dramatic below ∼3.7 T, where Ref. [22] reported a transition between a ferrimagnetic phase and a field-induced ICAFM phase. A discontinuity in the real and imaginary components of the susceptibility appears near 1.7 T, with the field value at which it occurs weakly depending on quench rate, possibly signifying the boundary of the frozen state. Despite corrections for the background coil, qualitative similarity in the high-field form of χ'
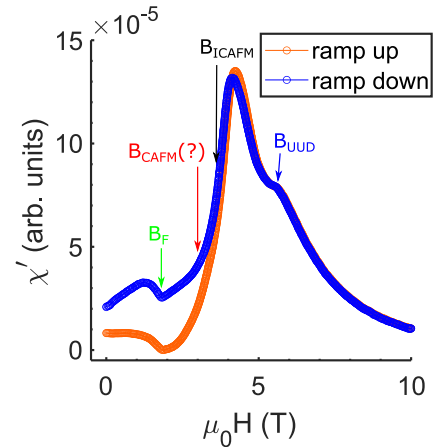

FIG. 3. Typical ac susceptibility data taken at $T = 0.5$ K as a function of transverse field for the real component of the susceptibility. For both increasing and decreasing fields, the field ramp rate was 2 T/min. A shoulder observed near 5.3 T (B_{UUD}) is consistent with the field-induced transition between the paramagnetic and an "up-up-down" (UUD) ferrimagnetic phase identified in Ref. [22], which approximately corresponds to the TFIM QCP. A small hysteresis (history dependence) is evident at this phase boundary, but it is more pronounced below ∼3.7 T (B_{ICAFM}), which is a field-induced first-order transition into the ICAFM state [22]. The transition into the CAFM state reported in Ref. [22] around 3 T (B_{CAFM}) is more difficult to observe in our susceptibility data, though a small kink in the decreasing real component can be observed. A ramp-rate-dependent discontinuity around ∼1.7 T (B_F) may represent the onset of the frozen phase.

and χ'' indicates a small mixing of the two components at higher fields was likely in our experiment (see Appendix B 2).

Accompanying the development of hysteresis, a slow relaxation is observed in the susceptibility. The slow relaxation is seen for all fields below the ICAFM transition (3.7 T) but becomes more pronounced below the CAFM and freezing transitions (<3 T) (see Appendix B 3). In the frozen state, it appears that it would persist well beyond our maximum measurement time (600 s after reaching zero field).

In zero field following a field quench, our time-dependent ac susceptibility is best fit to a logarithmic relaxation form:

$$\chi'(t) = a \ln \left(\frac{t - t_0}{\tau} \right) + c, \tag{2}$$

where a is a negative scale factor, t_0 is the onset time of the relaxation, τ is needed to make the argument of the logarithm dimensionless and may represent an intrinsic relaxation time scale, and c represents an offset that is partially due to a background contribution. The form shown in Eq. (2) produces an unbounded χ' for infinite time and thus cannot represent the full relaxation curve. We treat it as an early-time approximation for the relaxation, similar to the intermediate-time logarithmic relaxation proposed by Ref. [48]. Thus the c parameter also likely accounts for some of the late-time behavior of the relaxation. The functional form above provides a slightly better fit compared to a power-law relaxation, and likewise, the power law fit gives a low exponent ($-0.10 \pm$
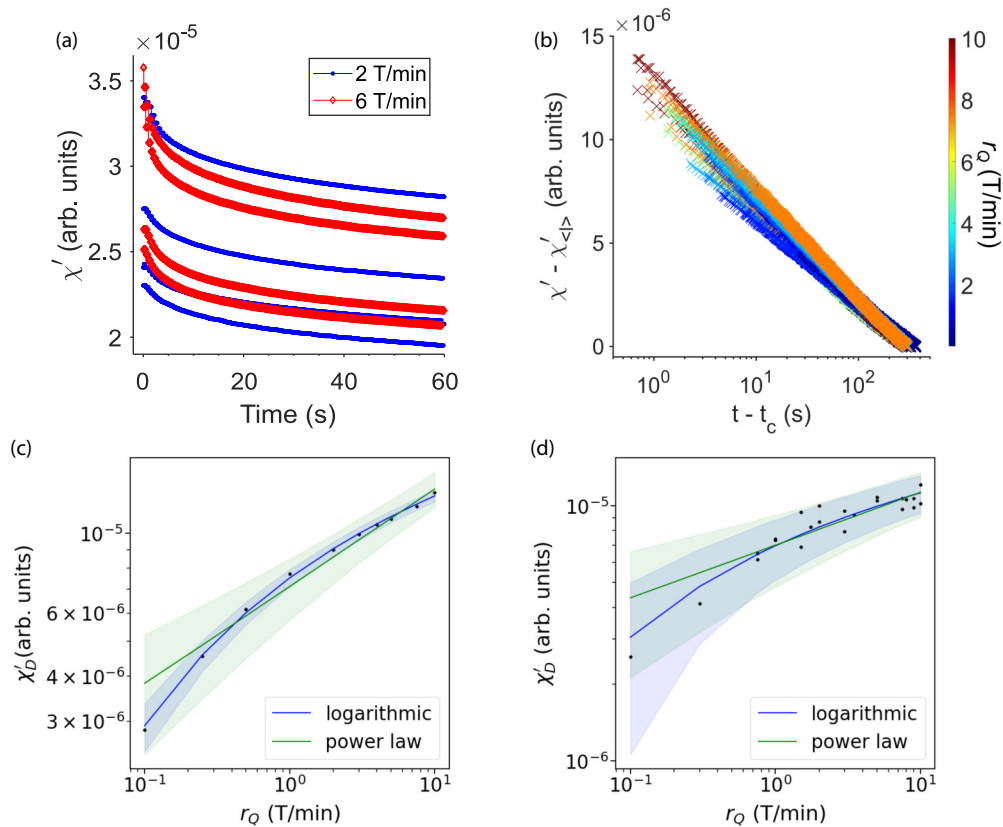
FIG. 4. (a) Relaxation of the magnetic susceptibility in zero field at $T = 0.5$ K after several quenches from a maximum field of 4 T. Data are shown for a few representative quenches for two different rates of the decreasing field (r_Q), 2 T/min in blue and 6 T/min in red. The zero-field relaxation of several quenches show a history dependence of the initial and final susceptibility, leading us to use the difference χ'_D as a measure of the relaxation at a given r_Q see Eq. (3). (b) Zero-field relaxation of 4 T quenches with a logarithmic time scale, where time is shifted by a critical time "t_c" defined as the time at which the field reaches 0.11 T. This produces straight lines, confirming the logarithmic form of relaxation, but indicating an unusually low field for the onset of relaxation. (c, d) χ'_D vs r_Q for a representative set of quenches (all completed after the same cooldown after warming past T_F) from a maximum field of (c) 4 T and (d) 6 T. The fits were performed using Bayesian nonlinear regression. The logarithmic form Eq. (5) arises from purely systematic effects, while the power-law form could potentially arise from the KZM. Shaded regions represent the 95% credible intervals of the posterior predictive distribution. For both sets of quenches, the logarithmic form gives the best fit.

0.03), hinting at the appropriateness of a logarithmic relaxation for our data (see Appendix B 4).

The zero-field power-law relaxation of ac susceptibility obtained in Ref. [25] was measured at 1.5 K, which is above T_F, and after different quench protocols compared to ours (they used temperature quenches and a c-axis field quench). We therefore do not necessarily expect the relaxation forms to agree, particularly if the frozen state is due to disorder. Indeed, disorder has been predicted to lead to logarithmic coarsening in Ising systems [49], while other studies have proposed a crossover from a power-law to a logarithmic form beyond a critical time related to the length scale separating impurities [41,50]. Slow relaxation in many systems, including spin glass systems, has also been modeled through hierarchically constrained dynamics [51–53]. Such a dynamical structure has been shown to lead to either a stretched exponential [54,55] or logarithmic [48] form of the relaxation.

C. Quench-rate dependence of susceptibility

One may think of the zero-field ac susceptibility as containing the response of the domain walls, as well as the intrinsic response of the CAFM ground state. Generally, we expect any signature which displays a relaxation over time to be partially attributed to the domain walls of the system (the units resulting from nonequilibrium). However, one intriguing observation we have made is the presence of aging effects, i.e., certain properties of the relaxation depend on the overall history since cooling into the frozen state, *even after* the transverse field is brought to 6 T, which is outside any ordered states. This is discussed in more detail in Appendix B 3 [also see Figs. 6(d) and 8]. While intriguing, this aging complicates the analysis of the quench rate dependence, since even identical repeated quenches lead to different offsets of the susceptibility, as shown in Fig. 4(a). To investigate the *trends* of the relaxation within the frozen state, we thus characterized the relaxation by the difference between its initial value and final value:

$$\chi'_D = \langle f \rangle - \langle l \rangle, \qquad (3)$$

where $\langle f \rangle$ describes the average of the first second of zero-field data after the quench and $\langle l \rangle$ is the average of the last second of collected data (usually at 300 s). This represents the initial density of defects due to each new quench. When

TABLE I. Fitted parameters for the quench-rate-dependent data and models shown in Figs. 4(c) and 4(d). Bracketed numbers indicate one standard deviation.

		4 T	6 T
Logarithmic	a_L	$2.30(6) \times 10^{-6}$	$1.9(2) \times 10^{-6}$
	B_c	0.20(2)	0.13(6)
Power law	a_p	$7.1(3) \times 10^{-6}$	$7.0(3) \times 10^{-6}$
	b	0.27(2)	0.21(3)

χ'_D is plotted as a function of quench rate (r_Q), a clear trend is seen [Figs. 4(c) and 4(d)]. In both crystals studied, this same type of dependence on quench rate was observed for all sets of quench data, which include quenches from 6 T across the QCP as well as quenches from 4 T which do not cross the QCP. Thus, the dependence on r_Q is not due to either the 1D or 3D QPT. Rather, it seems to be due to a very low field transition around 0.11 T, which is made evident by the analysis described in Appendix B 5. This field scale is also evident in the time-dependent data; when we shift the time axis by the time this field was reached (t_c), we see that $\chi'(t)$ is linear on a semilogarithmic scale [Fig. 4(b)]. This also further emphasizes the appropriateness of the logarithmic relaxation form Eq. (2) discussed above.

Turning to the quench-rate dependence of the difference in susceptibility, $\chi'_D(r_Q)$ [Figs. 4(c) and 4(d)], we used a Bayesian nonlinear regression to fit two models. The first is a power-law form,

$$\chi'_D(r_Q) = a_p r_Q^b, \tag{4}$$

where a_p is a scale factor, and b is the exponent. This was motivated by the fact that an almost-linear dependence of $\chi'_D(r_Q)$ appears on a log-log plot, and would potentially indicate KZM (see Appendix A for a discussion of the expected values for b for this scenario).

The second analytic form was derived considering a constant initial population of domain walls produced at a critical field B_c, which coarsen *during* the quenches before the field reaches zero (see Appendix B 5 for more details). This logarithmic form is

$$\chi'_D(r_Q) = a_L \ln \left[\frac{B_c/r_Q}{t_m + B_c/r_Q} \right], \tag{5}$$

where t_m is the measurement time between $\langle f \rangle$ and $\langle l \rangle$ (300 s for most quenches), a_L is a scale factor that would be expected to be the same a used in Eq. (2), and B_c is a fitting parameter describing the critical field at which relaxation starts.

Both forms result in a reasonable fit of the data, but the logarithmic form, which we refer to as "systematics" (since it does not involve any additional physics such as KZM), does better at the lowest quench rates. The means of the fitting parameters and their standard deviations of the parameters for the two models are shown in Table I, and details of the fitting procedure and resulting joint distributions of parameters are in Appendix B 5. We note that the $\chi'_D(r_Q)$ dependence of the 6-T quenches was significantly noisier than that of the 4-T quenches. The reason for this is currently unknown, but it was a reproducible effect during the experiments.

The power-law model would potentially indicate KZM, but with an unexpected scaling exponent of 0.27(2) for the 4-T data, and 0.21(3) for the 6-T data. The naively expected exponents are greater than 0.5, but they can be reduced due to coupling to a bath (see Appendix A). Yet, despite the predicted ubiquity for KZM across phase transitions, the logarithm explains our data better, as is evident from Fig. 4. The form of the logarithmic scaling can be completely understood to be a consequence of a systematic effect, namely, the coarsening of domains during the quench. Another way to see this is that the fitting parameter a in Eq. (2), which could reasonably be expected to scale with defect density, is independent of r_Q (see Appendix B 3).

Thus, it appears that we have not observed Kibble-Zurek scaling in this experiment, which is somewhat surprising, since it is expected to apply at all second-order phase transitions as well as glass transitions. One clue that may help to explain this is the low critical field ($B_c < 0.3$ T) inferred from the systematics analysis Eq. (5), which is well below any of the known phase transitions for a b-axis field applied to $CoNb_2O_6$ [22]. Further, the time associated with crossing this field is also the offset in time required to produce linear dependence of the susceptibility on a logarithmic time scale [Fig. 4(b)], i.e., t_c.

One possibility that could help to explain the low B_c, which also seems to explain the absence of Kibble-Zurek scaling, is that we are primarily observing the effects of a transition that is due to a small component of the field being within the ac plane, due to the slight misorientation of the sample (estimated to be about $1°$). Indeed, $CoNb_2O_6$ is known to exhibit a complex phase diagram when the field is applied in the ac plane, where several low-field transitions are first order in nature [13]. Thus, it may be that the dominant behavior observed in our quench-rate experiments is due to coarsening effects that occur after crossing a *first-order* phase transition induced by a small component of the field being applied in the ac plane, rather than a second-order or glass transition.

IV. CONCLUSION

In summary, we have performed ac susceptibility measurements of the quasi-1D Ising material $CoNb_2O_6$ in zero field and under predominantly transverse magnetic fields. At low temperature (0.5 K) we see evidence of several transverse-field-induced transitions at fields below the known QCP (at 5.3 T), some of which are similar to those which have been predicted theoretically [21] and observed in a prior study [22]. We have also observed and characterized a zero-field transition into an unconventional frozen state at $T_f = 1.2$ K, which is within the known commensurate antiferromagnetic state. This is consistent with earlier reports of extremely slow dynamics in this temperature range, but has not been discussed in detail before. Within this frozen state, the c-axis ac susceptibility shows a logarithmic relaxation over time in response to a transverse (b-axis) dc field quench. This form of relaxation is expected for coarsening of domains in the presence of disordered potentials, and this is an appealing explanation given prior work which successfully attributed some higher-temperature behavior of $CoNb_2O_6$ to domain-wall motion and coarsening [24,25]. However, the presence of lattice disorder

in our (and other group's) samples of $CoNb_2O_6$ remains to be confirmed.

We investigated the effect on the ac susceptibility response of "quenching" a transverse field across the various field-induced phase transitions of $CoNb_2O_6$. We found a surprising aging effect that indicates that the system is *not* reset by an applied field of 6 T, which is above the QPT within the "quantum paramagnetic" regime. After accounting for this aging effect, we do find a distinct dependence of χ' on quench rate, similar to a power-law scaling that would be expected based on the KZM. However, our observed dependence does not strongly depend on whether the QPT is crossed or not, and furthermore, we find it can be better fit by a logarithmic function arising from systematic effect, namely, coarsening *during* the field quench. Thus, we observe no evidence for the KZM in quenches across the QPT, or across any of the field-induced transitions including the freezing transition. Rather, the systematic analysis suggests that the observed effect is due to crossing a first-order transition brought about by a slight field misorientation.

This "null result" is somewhat surprising given the proposed ubiquity of the KZM phenomenon for second-order transitions (and generalized to glass transitions), and the fact that we clearly observe nonequilibrium states generated by the quenches. However, we cannot rule out that the Kibble-Zurek scaling is being obscured by the aging effect we have observed.

Overall, our results emphasize the complexity of the dynamical behavior of the well-studied quasi-1D transverse-field Ising model material $CoNb_2O_6$ under relatively weak transverse fields. This weak-transverse-field regime has until now not been explored in detail experimentally, but appears to contain a wealth of intriguing phenomena related to the frustration of the isosceles triangular lattice, which is likely to be strongly influenced by additional quantum fluctuations produced by the transverse field.

APPENDIX A: KIBBLE-ZUREK CONSIDERATIONS IN $CoNb_2O_6$

One goal of this study was to investigate the possibility of a Kibble-Zurek mechanism (KZM) in $CoNb_2O_6$. By quenching a control parameter through a continuous phase transition the system will inherently be driven out of equilibrium, a direct result of the divergence of the relaxation time near the critical point. This results in a nonzero density of defects which accumulate in the system for any finite quench rate. The density of defects, and all observables that depend on it, are predicted to scale as a power law with the quench rate, r_Q [6]. The density of defects, ρ, is predicted to scale as

$$\rho \sim r_Q^{d\nu/(1+z\nu)}, \tag{A1}$$

where r_Q is the quench rate, d is the dimension, ν is the correlation length critical exponent, and z is the dynamical critical exponent. The interest in Kibble-Zurek scaling is twofold. First, despite being an inherently nonequilibrium effect, which is typically challenging to describe, this phenomenon is described *entirely* by equilibrium properties (critical exponents). Second, the only requirement for Kibble-Zurek effects to occur is to cross a continuous phase transition at a finite rate, with the scaling relying only on the universality class of the system. While it was originally formulated by Kibble for defects in the early universe [57,58], it was extended to condensed matter systems by Zurek, who proposed it in superfluid helium [4]. It has since been generalized to quantum phase transitions [5,59,60], and experimental evidence for the KZM has been found in many systems including superfluid He [61], cold ion chains [62], and Bose condensates [63,64]. To this date, no scaling from a KZM due to a quantum phase transition has been observed in a magnetic system, where a magnetic field can provide a natural tuning parameter. Due to strong spin-lattice coupling, typical relaxations in magnetic systems are fast (picoseconds). However, the time scale for observation of defects is not limited by this spin-lattice relaxation; rather, it is limited by the coarsening time, which relies on the mobility of defects (to some extent set by the exchange interactions) and the dimension. Thus, one should expect that when defect motion is restricted, perhaps by disorder or frustration, KZ scaling could be readily observed over experimentally achievable time scales. To accurately assess the power-law exponent, observation of the scaling over several orders of magnitude of the quench rate is desirable. Conventional superconducting magnets are limited to slow quench rates ($< 10^{-1}$ T/min) and do not offer a reasonable range. Alternatively, resistive magnets can reach much higher magnetic field quench rates; the 31-T magnet at NHMFL provided us a range between 0.1 and 10 T/min. Ultrafast field ramps can also be achieved through pulsed magnets, which can reach quench rates of $> 10^3$ T/min [65,66].

The combination of an appropriate range of magnetic field quench rates as well as the observed slow coarsening dynamics of $CoNb_2O_6$ suggests it would have been a good candidate for observation of KZM. What is less obvious is what type of scaling should observed in $CoNb_2O_6$. It is well established that near the QCP $CoNb_2O_6$ displays hallmark behavior of the 1D TFIM with small but nonzero longitudinal field from the intrachain couplings [17,27,28]. In the case of defects being kinks along the Ising chains, scaling could be that of the QCP of the 1D Ising chain with an exponent of 0.5 [9,67]. However, $CoNb_2O_6$ orders into a 3D magnetically ordered ground state with much of its coarsening behavior at $T = 1.5$ K attributed to domain walls within the *ab* plane [24,25]. These defects would then perhaps be expected to scale according to the QCP of the 3D Ising model with an exponent of 0.75 [68,69]. With

a frozen state developing below $T_F = 1.2$ K, the system may be described better through a random Ising model, where dramatically increased dynamical exponents can greatly reduce expected scaling exponents.

These predictions also are only inherently true for closed quantum systems, which we know $CoNb_2O_6$ is *not*. Recent theoretical work for 1D Ising systems shows that coupling to a bosonic bath greatly reduces the critical exponent down to 0.28 [70]. Experimental work on quantum simulators of the 1D TFIM have also estimated the value of the scaling exponent due to the KZM range between 0.20 and 0.33 [71]. Coarsening and the KZM have been further explored [33], with estimates that in $d > 2$, coarsening does not strongly affect the expected critical exponents [32].

Finally, we note that the scaling of the initial ac susceptibility with quench rate, parametrized by a in Eq. (2), would likely be a good indicator of defect density. But as discussed in Appendix B 4 (and shown in Fig. 8), we find that a does not depend on quench rate systematically; rather, it appears to display some aging effects, though not as clearly as the c parameter.

APPENDIX B: TRANSVERSE-FIELD SUSCEPTIBILITY

1. Fine tuning of orientation

For conventional ac susceptibility, one measures with the ac field in the same direction as the dc field. In contrast, for the susceptometer we used, the ac component was measured along the crystallographic c axis, while the dc field could be applied anywhere in the bc plane by an *in situ* rotation of the ac coil set. The samples were loaded and aligned into the coil set with use of a Laue diffractometer, limiting a possible rotation of the sample out of the bc plane to 1°. In order to accurately align the dc field to be transverse to the Ising axis (i.e., b), we first located the c axis by rotating the coil set under a 1-T dc field through a range of angles for which the direction of H_{ac} is approximately equal to that of H_{dc}, and once determined, set the coil set to 90° from there. Figure 5(a) shows an approximately symmetric signal around "108°", which identifies the coil angle of 108° as the c-axis direction. The several peaks observed around this position are likely indicating different field-induced transitions as a function of angle (for fields near the Ising axis, the phase diagram is known to be highly complex [13,20]). The overall background from the coil is not symmetric, but this is likely due to details of the coil design and centering in the magnet.

2. Background subtraction

In general, for ac susceptometers in a transverse field, an anisotropic background signal of the coil can develop, which can be both field dependent and frequency dependent [72]. For our setup, an estimate of the coil background was taken using a high-temperature scan at 10 K, well into the paramagnetic phase [Fig. 5(b)]. This background is subtracted from all ac susceptibility figures shown. We note that during our experiment, the phase was taken at zero field and kept constant. Since the phase is expected to change as a function of magnetic field, it is possible that there is a small contribution of χ' appearing in χ'' in the paramagnetic phase. This
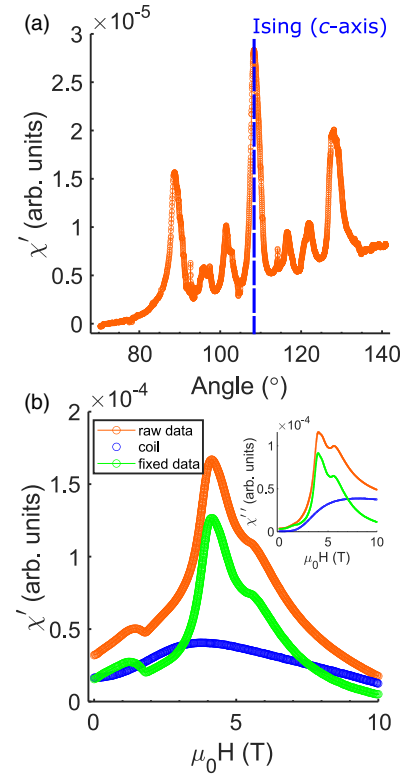

FIG. 5. (a) Real component of ac susceptibility vs linear motor rotation angle taken under a 1-T dc field. A large peak near 108° shows the location of the average Ising axis (c), which is identified based on the symmetric peaks around it, which likely relate to field-induced phase transitions that are highly dependent on the field direction. (b) Example of transverse-field-dependent susceptibility, with the background from coil shown, which was taken at 10 K for the real component (main figure) and imaginary component (inset) of the susceptibility. The background from the coil shows a frequency dependence as well as transverse-field dependence but little to no quench-rate dependence at 710 Hz (not shown).

would naturally explain the similar qualitative forms of the components in field, as well as the nonvanishing value of χ'' at 10 T.

3. Aging effects

In an attempt to separate any possible trends coming from aging effects compared to quench-rate effects, we instituted the following protocol for our magnetic field quenches: after the system was reset (warmed to 1.8 K then cooled in zero field), we ran a series of quenches from 0 T up to a maximum field (either 6 or 4 T) and then back down to 0 T. Each of the quench protocols consisted of an identical field sweep rate of 1 T/min from zero up to the maximum field, a hold at the maximum field for 10 s, and a field sweep (quench) rate chosen to be between 0.1 and 10 T/min for the quench back to 0 T. The system was then reset again before another set of quenches by warming above T_F. By doing the quenches "out of order" with respect to quench rate, we are able to separate any overall aging effects (i.e., effects that correlate with run number, which loosely represents time since cooling into the frozen state) from effects depending on the quench rate, r_Q.
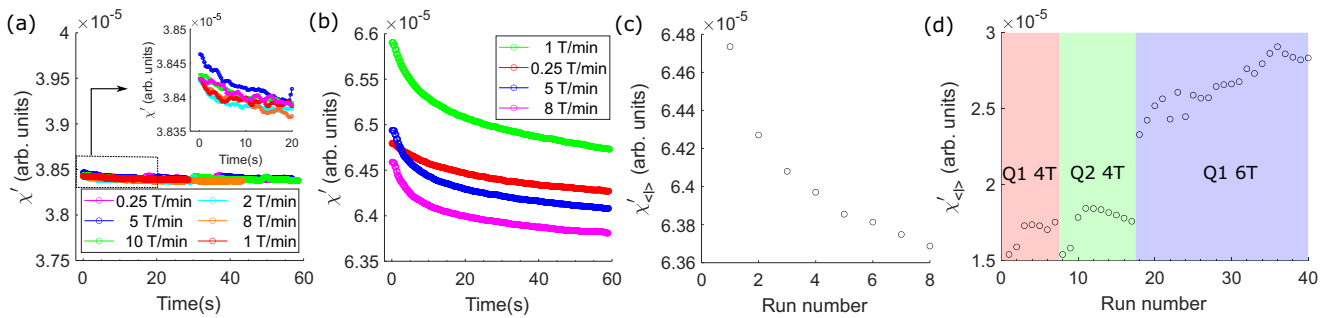
FIG. 6. (a, b) Representative ac susceptibility data taken at the end of intermediate (stepwise) quenches for various points in the phase diagram. Both panels are set to the same scale to compare size of the relaxation. (a) 4-T to 3-T quenches showing a small relaxation barely larger than instrument noise limit, showing the approach to the CAFM state near 3 T. (b) 3-T to 2-T quenches show a clear relaxation well beyond the noise limit. (c) Average susceptibility over last second of measuring time ($\chi'_{\langle l \rangle}$) as function of quench run number for data in panel (b). Above the frozen transition, the system relaxes overall with each subsequent quench. (d) Average susceptibility over last second of measuring time ($\chi'_{\langle l \rangle}$) as function of quench data for zero-field data showing aging effects within frozen state. Q1 4T and Q2 4T show two separate sets of quenches with a maximum field of 4 T, while Q1 6T shows a set of quenches following a maximum field of 6 T.

To observe at what field the relaxation begins, we measured the susceptibility over time for many smaller intermediate magnetic field quenches (e.g., 4 to 3 T, 3 to 2 T, etc.). A small relaxation on the order of the noise limit of our experiment is observed in the 4-T to 3-T quenches, shown in Fig. 6(a). The onset of appreciable relaxation occurs for quenches from 3 to 2 T, across the previously identified transition between the ICAFM and CAFM ordered states at ~3 T [Fig. 6(b)]. For the final fields above the freezing transition, relaxations show an overall aging effect such that progressive quenches are shifted down with run number [Fig. 6(c)]. For final fields below the anomaly at $B_f \sim 1.7$ T, which we have tentatively associated with a field boundary of the frozen phase, the relaxation gains a more complicated dependence on the quench rate, shown in the main text by the zero-field relaxation [Fig. 4(a)]. Looking at the average susceptibility at the last second of measurement time, shown in Fig. 6(d), we notice two different aging behaviors in the 4-T and 6-T quenches. For the 4-T quenches, the average final susceptibility increases with initial runs and then saturates, while the 6-T quenches increase with consecutive quenches. Any trend that appears as a function of run number (which was not correlated with quench rate, by design) strongly suggests aging effects are present, and we find that these are surprisingly *not erased* by going to 6 T (in the paramagnetic regime). This may be related to the presence of significant energy dissipation up to 10 T, as indicated by the high χ'' (Fig. 3) at 6 T, and suggests that one needs to go to higher fields to reset the system.

In order to account for the aging effect, which mainly seemed to produce an offset to χ', we looked at the difference of the first second and last second of the susceptibility, χ'_D Eq. (3).

4. Analysis of time dependence of χ'

After a magnetic field quench (i.e., when the dc field returns to zero), we observe a decay over time of the real and imaginary components of the susceptibility at $T = 0.5$ K; i.e., a nonequilibrium state is generated. This decay appears for all quenches to zero field, regardless of their starting field values (which were either 4 or 6 T), indicating that the

nonequilibrium state is not due to quenching through the QPT associated with the 1D TFIM (at 5.2 T) or the 3D QPT to the field-polarized paramagnet (at 5.4 T).

Following a field quench at 0.5 K, the time dependence of the zero-field relaxation within the frozen state can be fit relatively well to three different forms: a stretched exponential, a power-law decay, and a logarithmic function given by

$$\chi'(t, B = 0) = a \exp\left[-\left(\frac{t - t_0}{\tau}\right)^{\beta}\right] + c, \quad \text{(B1a)}$$

$$\chi'(t, B = 0) = a\left(\frac{t - t_0}{\tau}\right)^{n} + c, \quad \text{(B1b)}$$

$$\chi'(t, B = 0) = a \ln\left(\frac{t - t_0}{\tau}\right) + c, \quad \text{(B1c)}$$

respectively. In each of the forms, t_0 represents the time of relaxation onset, τ represents an intrinsic time (needed in theory to make the time arguments dimensionless, but absorbed into the other parameters for fitting purposes), a is a scale factor that one could expect to represent the initial population of defects generated by the quench, and c is an offset due to late-time behavior and/or background. For the stretched exponential, τ represents the average relaxation time and β represents the distribution of relaxation times. This form of relaxation is commonly found in glass systems [73,74], and has also been found for hierarchically constrained dynamics [54]. A power law would instead indicate relaxations occurring on all time scales with growth exponent n describing the coarsening. Power-law relaxation has been observed for $CoNb_2O_6$ at higher temperature above the glass transition where the exponent n was found to be -0.2 [24,25,47]. Meanwhile, the logarithmic relaxation function has also been proposed for hierarchical dynamics [48], and is often seen for domain coarsening in disordered models, such as the random-field Ising model [75,76].

To determine the best model for the decay, we compared χ^2 for fits of the three models to several relaxation curves. An example of best fits for the three functional forms are shown in Fig. 7, where the best-fit parameters used are shown in Table II. Note that the form of the power-law and logarithmic
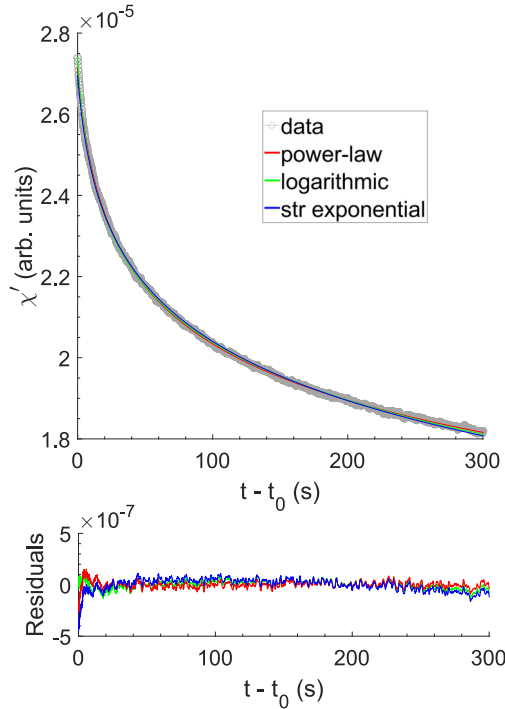
FIG. 7. Example of least-squares best fits to zero-field relaxation for the following functional forms: power law, stretched exponential, and logarithmic decay.

decay functions have absorbed τ into the definition of the other parameters, a and c, as appropriate. For the sake of comparison to Refs. [24,25], we note the data can be well represented by a power law, but with a smaller exponent of $n = -0.097(3)$ compared to the value reported in literature ($n = -0.2$). While the χ^2 for the three forms were comparable, in the end we chose the logarithmic form due to the reduced number of free parameters required to accurately fit the decay, and the very small exponent indicated by the power-law fit.

From intermediate quench data (quenches ending at a nonzero field), the system only shows a sizable decaying population below the CAFM transition, $B_{CAFM} \sim 3$ T. Within

TABLE II. Table of least-squares fits to typical zero-field relaxation of the susceptibility of $CoNb_2O_6$ at $T = 0.5$ K taken after a 2 T/min quench from a peak field of 4 T. Best fit parameters are shown for three different forms of the relaxation: a logarithmic relaxation, a power-law relaxation, and a stretched exponential relaxation. τ was absorbed into a and c for the power-law and logarithmic forms, respectively, in order to reduce free parameters.

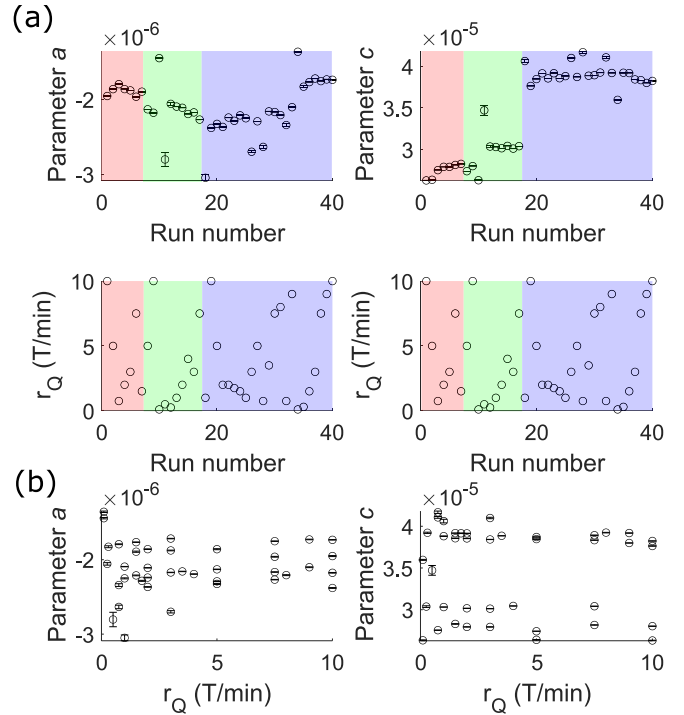|	Logarithmic $a\ln(t - t_0) + c$	Power law $a(t - t_0)^n + c$	Stretched exponential $a\exp[-(\frac{t - t_0}{\tau})^\beta] + c$
a	$-2.11(2) \times 10^{-6}$	$3.54(6) \times 10^{-5}$	$3.9(5) \times 10^{-4}$
t_0	$368.6(2)$	$365.3(4)$	$367(1)$
c	$3.02(1) \times 10^{-5}$	$-2.2(8) \times 10^{-6}$	$-1.2(3) \times 10^{-4}$
n		$-0.097(3)$	
τ			$124(8)$
β			$0.01(5)$
χ^2	3.2×10^{-6}	2.3×10^{-6}	7.0×10^{-6}

FIG. 8. (a) Best fit parameters a and c for least-squares fit of Eq. (B1c) as a function of quench run number, shown with pseudorandom r_Q protocol as a function of quench run number. Color overlays show distinct sets of quenches: red is Q1 4T, green is Q2 4T, and blue is Q1 6T. Parameters a and c both show weak trends in run number, suggesting aging. Parameter c also shows a general offset to the data for each individual quench set (each set started after warming past T_f and cooling back down in zero field). (b) Plots of best-fit parameters a and c for least-squares fit of Eq. (B1c) as a function of r_Q, where errors plotted are 95% confidence intervals of the fitted parameters. Although the spread in values is much larger than the error bars, they show no obvious dependence on ramp rate.

the frozen state, best-fit values of the parameters a and c show a large distribution of values, but remain largely insensitive to the quench rate of the magnet, shown in Fig. 8.

5. Quench rate dependence of χ'_D

During our experiments, the magnetic field was decreased linearly at a set quench rate from 6 T down to 0 T and from 4 T down to 0 T, as well as between intermediate field values, as described above. The quench rate, r_Q, is given by

$$r_Q = \frac{dB}{dt},$$
$$r_Q = \frac{B_i - B_f}{t_i - t_f}, \qquad \text{(B2)}$$

where the subscripts i and f refer to the initial and final parameters of the quench. Note that r_Q is defined to be positive for a decreasing field. In order to analyze the r_Q dependence of χ'_D, we considered two analytical forms. The first is a power law, which would be potentially consistent with KZM [Eq. (4) in the main text, repeated here],

$$\chi'_D(r_Q) = a_p r_Q^b, \qquad \text{(B3)}$$

TABLE III. Prior distributions for the model parameters used in the Bayesian regression. ϵ is the standard deviation associated with the normal distribution of the data away from the mean (best-fit line). We chose a half-normal distribution centered at zero since the standard deviation cannot be negative.

	4 T	6 T
Logarithmic	a: Unif$(0, 5 \times 10^{-6})$ B_c: Unif$(0, 3)$ ϵ: HalfNormal$(\sigma = 1 \times 10^{-5})$	a: Unif$(0, 5 \times 10^{-6})$ B_c: Unif$(0, 3)$ ϵ: HalfNormal$(\sigma = 1 \times 10^{-5})$
Power law	a: Unif$(0, 40 \times 10^{-6})$ b: Unif$(0, 2)$ ϵ: HalfNormal$(\sigma = 5)$	a: Unif$(0, 40 \times 10^{-6})$ b: Unif$(0, 2)$ ϵ: HalfNormal$(\sigma = 5)$

where a_p is a scale factor depending on the overall number of defects generated by the quenches, and b is the power-law exponent. The expected values for b are discussed in Appendix A.

A second analytic form accounts for the effects of domain coarsening during the quench. This will occur for any open system where coarsening occurs on the same approximate time scale as the quench time. We refer to the results of coarsening during the quench as a "systematic effect" since it does not require any additional physics such as the KZM. To derive the analytic expression we assumed that the coarsening or relaxation takes place with an identical form throughout the field range below the relevant transition, following Eq. (2) (the logarithmic relaxation form). We find that this systematic effect would lead to the following $\chi'_D(r_Q) = \langle f \rangle - \langle l \rangle$ form at zero field [Eq. (5) presented in the main text, repeated here}:

$$\chi'_D(r_Q) = a \ln \left[\frac{B_c/r_Q}{t_m + B_c/r_Q} \right], \qquad \text{(B4)}$$

where t_m is the measurement time between the first few sections of the measured zero-field relaxation (over which χ' is averaged to produce $\langle f \rangle$) and the last few seconds (over which χ' is averaged to produce $\langle l \rangle$); t_m was 300 s (5 min) for all of our data presented here. Meanwhile, a is in principle the same scale factor as in Eq. (2) [though we let it be a free parameter in our analysis and compared to the results of fitting Eq. (2) afterwards], and B_c is a fitting parameter describing the critical field at which relaxation starts.

We performed a Bayesian nonlinear regression analysis of one set of 4-T quench data and one set of 6-T data. The analysis was performed using the Markov chain Monte Carlo package PYMC3 [77] for PYTHON. For our prior distributions, we used *uniform* distributions for most parameters, with limits as indicated in Table III, except for the random error parameter (which accounts for the standard deviation of the data points away from the mean value predicted by the model), for which we used half-normal distribution. The iPython notebook used to complete the analysis is available in the Supplemental Material [78].

We chose to use a Bayesian approach because we encountered great difficulty in reliably fitting Eqs. (B3) and (B4)
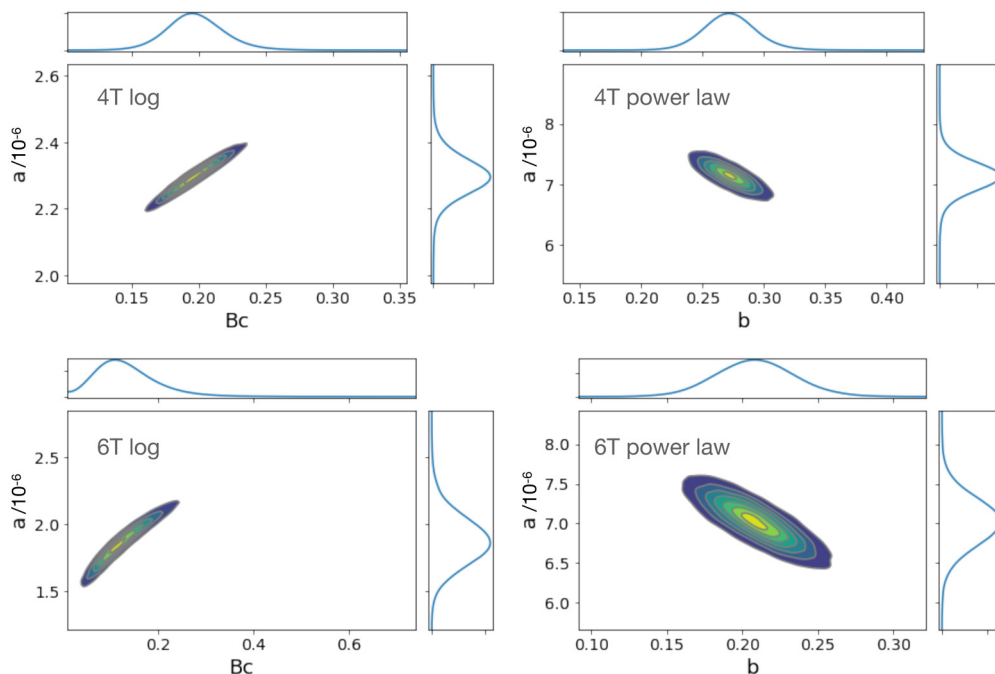

FIG. 9. Joint distributions of the parameters for the two models fit to the $\chi'_D(r_Q)$ data.

using a traditional least-squares (maximum likelihood estimation) approach, and suspected it was due to highly correlated parameters. The advantage of Bayesian regression is that it gives access to the joint probability distribution of the model parameters, which can be inspected directly to understand the nature of the correlations (these are shown in Fig. 9 for the analyses discussed here). The joint distributions for both models reveal that the parameters in question are correlated, as expected based on the difficulty of fitting using a least-squares approach, but they are unimodal, and clear maxima can be identified.

Another advantage of Bayesian analysis is that it allows for a more complete understanding of the uncertainties of the fitted models. These are indicated by the 95% credible intervals of the mean of the posterior distributions, shown as shaded colored areas in Figs. 4(c) and 4(d). The results of this analysis indicate that the logarithmic model works best for both 4-T and 6-T quenches, in that it produces a more certain posterior predictive distribution. This is particularly visible for the 4-T quenches, where the 95% credible interval (shaded blue area) is narrower for the whole range of quench rates compared to the power-law model.

[1] A. Pal and D. A. Huse, Many-body localization phase transition, Phys. Rev. B **82**, 174411 (2010).

[2] R. Nandkishore and D. A. Huse, Many-body localization and thermalization in quantum statistical mechanics, Annu. Rev. Condens. Matter Phys. **6**, 15 (2015).

[3] M. Friesdorf, A. H. Werner, W. Brown, V. B. Scholz, and J. Eisert, Many-Body Localization Implies that Eigenvectors are Matrix-Product States, Phys. Rev. Lett. **114**, 170505 (2015).

[4] W. H. Zurek, Cosmological experiments in superfluid helium? Nature (London) **317**, 505 (1985).

[5] J. Dziarmaga, Dynamics of a Quantum Phase Transition: Exact Solution of the Quantum Ising Model, Phys. Rev. Lett. **95**, 245701 (2005).

[6] A. Chandran, A. Erez, S. S. Gubser, and S. L. Sondhi, Kibble-Zurek problem: Universality and the scaling limit, Phys. Rev. B **86**, 064304 (2012).

[7] P. Pfeuty, The one-dimensional Ising model with a transverse field, Ann. Phys. **57**, 79 (1970).

[8] R. Elliott, P. Pfeuty, and C. Wood, Ising Model with a Transverse Field, Phys. Rev. Lett. **25**, 443 (1970).

[9] A. Dutta, G. Aeppli, B. K. Chakrabarti, U. Divakaran, T. F. Rosenbaum, and D. Sen, *Quantum Phase Transitions in Transverse Field Spin Models: From Statistical Physics to Quantum Information* (Cambridge University Press, Cambridge, UK, 2015).

[10] I. Maartense, I. Yaeger, and B. Wanklyn, Field-induced magnetic transitions of $CoNb_2O_6$ in the ordered state, Solid State Commun. **21**, 93 (1977).

[11] W. Scharf, H. Weitzel, I. Yaeger, I. Maartense, and B. Wanklyn, Magnetic structures of $CoNb_2O_6$, J. Magn. Magn. Mater. **13**, 121 (1979).

[12] T. Hanawa, M. Ishikawa, and K. Miyatani, Disappearance of ferromagnetism at low temperatures in $CoNb_2O_6$, J. Phys. Soc. Jpn. **61**, 4287 (1992).

[13] T. Hanawa, K. Shinkawa, M. Ishikawa, K. Miyatani, K. Saito, and K. Kohn, Anisotropic specific heat of $CoNb_2O_6$ in magnetic fields, J. Phys. Soc. Jpn. **63**, 2706 (1994).

[14] C. Heid, H. Weitzel, P. Burlet, M. Bonnet, W. Gonschorek, T. Vogt, J. Norwig, and H. Fuess, Magnetic phase diagram of $CoNb_2O_6$: A neutron diffraction study, J. Magn. Magn. Mater. **151**, 123 (1995).

[15] S. Kobayashi, S. Mitsuda, K. Hosoya, H. Yoshizawa, T. Hanawa, M. Ishikawa, K. Miyatani, K. Saito, and K. Kohn, Competition between the inter-chain interaction and single-ion anisotropy in $CoNb_2O_6$, Phys. B: Condens. Matter **213**, 176 (1995).

[16] C. Heid, H. Weitzel, P. Burlet, M. Winkelmann, H. Ehrenberg, and H. Fuess, Magnetic phase diagrams of $CoNb_2O_6$, Phys. B: Condens. Matter **234**, 574 (1997).

[17] R. Coldea, D. Tennant, E. Wheeler, E. Wawrzynska, D. Prabhakaran, M. Telling, K. Habicht, P. Smeibidl, and K. Kiefer, Quantum criticality in an Ising chain: Experimental evidence for emergent E_8 symmetry, Science **327**, 177 (2010).

[18] H. Weitzel, Kristallstrukturverfeinerung von wolframiten und columbiten, Z. Kristallogr. -Cryst. Mater. **144**, 238 (1976).

[19] S. Mitsuda, K. Hosoya, T. Wada, H. Yoshizawa, T. Hanawa, M. Ishikawa, K. Miyatani, K. Saito, and K. Kohn, Magnetic ordering in one-dimensional system $CoNb_2O_6$ with competing interchain interactions, J. Phys. Soc. Jpn. **63**, 3568 (1994).

[20] S. Kobayashi, S. Mitsuda, M. Ishikawa, K. Miyatani, and K. Kohn, Three-dimensional magnetic ordering in the quasi-one-dimensional Ising magnet $CoNb_2O_6$ with partially released geometrical frustration, Phys. Rev. B **60**, 3331 (1999).

[21] S. Lee, R. K. Kaul, and L. Balents, Interplay of quantum criticality and geometric frustration in columbite, Nat. Phys. **6**, 702 (2010).

[22] E. M. da Silva Wheeler, Neutron scattering from low-dimensional quantum magnets, Ph.D. thesis, University of Oxford, 2007.

[23] T. Liang, S. M. Koohpayeh, J. W. Krizan, T. M. McQueen, R. J. Cava, and N. P. Ong, Heat capacity peak at the quantum critical point of the transverse Ising magnet $CoNb_2O_6$, Nat. Commun. **6**, 7611 (2015).

[24] S. Kobayashi, S. Mitsuda, T. Jogetsu, J. Miyamoto, H. Katagiri, and K. Kohn, Anisotropic growth kinetics in the geometrically frustrated isosceles triangular Ising antiferromagnet $CoNb_2O_6$, Phys. Rev. B **60**, R9908 (1999).

[25] S. Kobayashi, H. Okano, T. Jogetsu, J. Miyamoto, and S. Mitsuda, Domain growth kinetics in the isosceles triangular Ising antiferromagnet $CoNb_2O_6$, Phys. Rev. B **69**, 144430 (2004).

[26] A. B. Zamolodchikov, Integrals of motion and S-matrix of the (scaled) $T = T_i c$ Ising model with magnetic field, Int. J. Mod. Phys. A **4**, 4235 (1989).

[27] S. Rutkevich, On the weak confinement of kinks in the one-dimensional quantum ferromagnet $CoNb_2O_6$, J. Stat. Mech.: Theory Exp. (2010) P07015.

[28] J. A. Kjäll, F. Pollmann, and J. E. Moore, Bound states and E_8 symmetry effects in perturbed quantum Ising chains, Phys. Rev. B **83**, 020407(R) (2011).

[29] A.W. Kinross, M. Fu, T.J. Munsie, H.A. Dabkowska, G.M. Luke, S. Sachdev, and T. Imai, Evolution of Quantum

Fluctuations near the Quantum Critical Point of the Transverse Field Ising Chain System CoNb$_2$O$_6$, Phys. Rev. X **4**, 031008 (2014).

[30] M. Fava, R. Coldea, and S. Parameswaran, Glide symmetry breaking and Ising criticality in the quasi-1D magnet CoNb$_2$O$_6$, Proc. Natl. Acad. Sci. USA **117**, 25219 (2020).

[31] C. Morris, N. Desai, J. Viirok, D. Huvonen, U. Nagel, T. Room, J. Krizan, R. Cava, T. McQueen, S. Koohpayeh *et al.*, Duality and domain wall dynamics in a twisted Kitaev chain, Nat. Phys. **17**, 832 (2021).

[32] G. Biroli, L. F. Cugliandolo, and A. Sicilia, Kibble-Zurek mechanism and infinitely slow annealing through critical points, Phys. Rev. E **81**, 050101(R) (2010).

[33] G. Biroli, Slow relaxations and non-equilibrium dynamics in classical and quantum systems, arXiv:1507.05858.

[34] C.-W. Liu, A. Polkovnikov, A. W. Sandvik, and A. P. Young, Universal dynamic scaling in three-dimensional Ising spin glasses, Phys. Rev. E **92**, 022128 (2015).

[35] N. Xu, K.-H. Wu, S. J. Rubin, Y.-J. Kao, and A. W. Sandvik, Dynamic scaling in the two-dimensional Ising spin glass with normal-distributed couplings, Phys. Rev. E **96**, 052102 (2017).

[36] B. Wanklyn, B. Garrard, and G. Garton, Flux growth of crystals of MNb$_2$O$_6$ (m = Ni, Co, Mn, Fe), Mater. Res. Bull. **11**, 1497 (1976).

[37] 31 T, 50-mm bore magnet (cell 9), maglab, https://nationalmaglab.org/user-facilities/dc-field/instruments-dcfield/resistive-magnets/31-tesla-cell-9.

[38] J. Lashley, M. Hundley, A. Migliori, J. Sarrao, P. Pagliuso, T. Darling, M. Jaime, J. Cooley, W. Hults, L. Morales *et al.*, Critical examination of heat capacity measurements made on a quantum design physical property measurement system, Cryogenics **43**, 369 (2003).

[39] H. Suzuki, A. Inaba, and C. Meingast, Accurate heat capacity data at phase transitions from relaxation calorimetry, Cryogenics **50**, 693 (2010).

[40] I. Lifshitz, Kinetics of ordering during second-order phase transitions, Sov. Phys. JETP **15**, 939 (1962).

[41] D. Chowdhury and S. Kumar, Domain growth in the three-dimensional dilute Ising model, J. Stat. Phys. **49**, 855 (1987).

[42] M. Cheon and I. Chang, Anisotropic Domain Growth of the Axial Next-Nearest-Neighbor Ising Model at Low Temperatures, Phys. Rev. Lett. **86**, 4576 (2001).

[43] A. Burdese, M. Borlera, and P. Rolando, Systems between niobium oxides and the oxides of nickel and cobalt, Atti Accad. Sci. Torino: I. Classe Sci. Fis., Mat. Nat. **99**, 565 (1964).

[44] J. Maier, Defect chemistry: Composition, transport, and reactions in the solid state; part I: Thermodynamics, Angew. Chem., Int. Ed. Engl. **32**, 313 (1993).

[45] Care must also be taken to convert cobalt oxide precursors to a single type. When purchased from chemical suppliers they often contain a mixture of Co$_3$O$_4$ and CoO which, if uncorrected, can lead to inaccurate Co stoichiometry.

[46] P. W. C. Sarvezuk, E. J. Kinast, C.V. Colin, M. A. Gusmao, J. B. M. da Cunha, and O. Isnard, Suppression of magnetic ordering in quasi-one-dimensional Fe$_x$Co$_{1-x}$Nb$_2$O$_6$ compounds, Phys. Rev. B **83**, 174412 (2011).

[47] T. Nakajima, S. Mitsuda, Y. Inomoto, K. Prokes, V. Sikolenko, S. Gerischer, and S. Kobayashi, Magnetic domain growth in geometrically frustrated Ising antiferromagnets Co$_{1-x}$Mg$_x$Nb$_2$O$_6$ (x = 0 and 0.004) as seen via time-resolved neutron diffraction measurements, Phys. Rev. B **90**, 064431 (2014).

[48] J. J. Brey and A. Prados, Slow logarithmic relaxation in models with hierarchically constrained dynamics, Phys. Rev. E **63**, 021108 (2001).

[49] D. A. Huse and C. L. Henley, Pinning and Roughening of Domain Walls in Ising Systems due to Random Impurities, Phys. Rev. Lett. **54**, 2708 (1985).

[50] D. Chowdhury, M. Grant, and J.D. Gunton, Interface roughening and domain growth in the dilute Ising model, Phys. Rev. B **35**, 6792 (1987).

[51] S. R. McKay, A. N. Berker, and S. Kirkpatrick, Amorphously packed, frustrated hierarchical models: Chaotic rescaling and spin-glass behavior, J. Appl. Phys. **53**, 7974 (1982).

[52] G. Hed, A. K. Hartmann, D. Stauffer, and E. Domany, Spin Domains Generate Hierarchical Ground State Structure in j = ±1 Spin Glasses, Phys. Rev. Lett. **86**, 3148 (2001).

[53] M. Castellana, A. Decelle, S. Franz, M. Mézard, and G. Parisi, Hierarchical Random Energy Model of a Spin Glass, Phys. Rev. Lett. **104**, 127206 (2010).

[54] R. G. Palmer, D. L. Stein, E. Abrahams, and P. W. Anderson, Models of Hierarchically Constrained Dynamics for Glassy Relaxation, Phys. Rev. Lett. **53**, 958 (1984).

[55] M. A. Munoz, A. Gabrielli, H. Inaoka, and L. Pietronero, Hierarchical model of slow constrained dynamics, Phys. Rev. E **57**, 4354 (1998).

[56] K. Momma and F. Izumi, VESTA: A three-dimensional visualization system for electronic and structural analysis, J. Appl. Crystallogr. **41**, 653 (2008).

[57] T. W. Kibble, Topology of cosmic domains and strings, J. Phys. A: Math. Gen. **9**, 1387 (1976).

[58] T. W. Kibble, Some implications of a cosmological phase transition, Phys. Rep. **67**, 183 (1980).

[59] W. H. Zurek, U. Dorner, and P. Zoller, Dynamics of a Quantum Phase Transition, Phys. Rev. Lett. **95**, 105701 (2005).

[60] A. Polkovnikov, Universal adiabatic dynamics in the vicinity of a quantum critical point, Phys. Rev. B **72**, 161201(R) (2005).

[61] P. Hendry, N. S. Lawson, R. Lee, P. V. McClintock, and C. Williams, Generation of defects in superfluid ^{4}He as an analogue of the formation of cosmic strings, Nature (London) **368**, 315 (1994).

[62] S. Ulm, J. Roßnagel, G. Jacob, C. Degünther, S. T. Dawkins, U. G. Poschinger, R. Nigmatullin, A. Retzker, M. B. Plenio, F. Schmidt-Kaler *et al.*, Observation of the Kibble-Zurek scaling law for defect formation in ion crystals, Nat. Commun. **4**, 2290 (2013).

[63] G. Lamporesi, S. Donadello, S. Serafini, F. Dalfovo, and G. Ferrari, Spontaneous creation of Kibble-Zurek solitons in a Bose-Einstein condensate, Nat. Phys. **9**, 656 (2013).

[64] M. Anquez, B. A. Robbins, H. M. Bharath, M. Boguslawski, T. M. Hoang, and M. S. Chapman, Quantum Kibble-Zurek Mechanism in a Spin-1 Bose-Einstein Condensate, Phys. Rev. Lett. **116**, 155301 (2016).

[65] L. Campbell, H. Boenig, D. Rickel, J. Schillig, H. Schneider-Muntau, and J. Sims, The NHMFL long-pulse magnet system: 60–100 T, Phys. B: Condens. Matter **216**, 218 (1996).

[66] 60 T, controlled waveform magnet, https://nationalmaglab.org/user-facilities/pulsed-field-facility/instruments-pff/60-tesla-controlled-waveform-magnet.

[67] V. Mukherjee, U. Divakaran, A. Dutta, and D. Sen, Quenching dynamics of a quantum *XY* spin-1/2 chain in a transverse field, Phys. Rev. B **76**, 174303 (2007).

[68] G. P. Zheng and J. X. Zhang, Determination of dynamical critical exponents from hysteresis scaling, Phys. Rev. E **58**, R1187 (1998).

[69] H. W. J. Blöte and R. H. Swendsen, Critical behavior of the four-dimensional Ising model, Phys. Rev. B **22**, 4481 (1980).

[70] H. Oshiyama, N. Shibata, and S. Suzuki, Kibble-Zurek mechanism in a dissipative transverse Ising chain, J. Phys. Soc. Jpn. **89**, 104002 (2020).

[71] Y. Bando, Y. Susa, H. Oshiyama, N. Shibata, M. Ohzeki, F. J. Gómez-Ruiz, D. A. Lidar, S. Suzuki, A. del Campo, and H. Nishimori, Probing the universality of topological defect formation in a quantum annealer: Kibble-Zurek mechanism and beyond, Phys. Rev. Research **2**, 033369 (2020).

[72] F. Rucker and C. Pfleiderer, Compact susceptometer for studies under transverse field geometries at very low temperatures, Rev. Sci. Instrum. **90**, 073903 (2019).

[73] J. C. Mauro and Y. Z. Mauro, On the Prony series representation of stretched exponential relaxation, Physica A **506**, 75 (2018).

[74] M. Potuzak, R. C. Welch, and J. C. Mauro, Topological origin of stretched exponential relaxation in glass, J. Chem. Phys. **135**, 214502 (2011).

[75] D. S. Fisher, P. Le Doussal, and C. Monthus, Nonequilibrium dynamics of random field Ising spin chains: Exact results via real space renormalization group, Phys. Rev. E **64**, 066107 (2001).

[76] F. Corberi, Coarsening in inhomogeneous systems, C. R. Phys. **16**, 332 (2015).

[77] PYMC3 probabilistic programming in python to be published.

[78] See Supplemental Material at http://link.aps.org/supplemental/10.1103/PhysRevB.104.214424 for an ipython notebook where the parameters quoted in the main paper are computed, as well as the two data files used in the notebook.